

## Simulation, bifurcation, and stability analysis of a SEPIC converter controlled with ZAD

Aquiles J. Morelo<sup>1</sup>, Simeón Casanova Trujillo<sup>2</sup>, Fredy E. Hoyos<sup>3</sup>

<sup>1,2</sup>Grupo de investigación: Cálculo Científico y Modelamiento Matemático,  
Universidad Nacional de Colombia - Sede Manizales, Colombia

<sup>3</sup>Faculty of Science, School of Physics, Universidad Nacional de Colombia-Sede Medellín,  
Carrera 65 Nro. 59A-110, Medellín 050034, Colombia

---

### Article Info

#### Article history:

Received Jun 11, 2019

Revised Sep 30, 2019

Accepted Oct 7, 2019

---

#### Keywords:

Bifurcation

Non-linear phenomena

SEPIC converter

ZAD technique

---

### ABSTRACT

This article presents some results of SEPIC converter dynamics when controlled by a center pulse width modulator controller (CPWM). The duty cycle is calculated using the ZAD (Zero Average Dynamics) technique. Results obtained using this technique show a great variety of non-linear phenomena such as bifurcations and chaos, as parameters associated with the switching surface. These phenomena have been studied in the present paper in numerical form. Simulations were done in MATLAB.

Copyright © 2020 Institute of Advanced Engineering and Science.  
All rights reserved.

---

### Corresponding Author:

Fredy E. Hoyos,

Facultad de Ciencias - Escuela de Física,

Universidad Nacional de Colombia - Sede Medellín,

Carrera 65 No. 59A-110, Medellín, Colombia.

Email: fehoyosve@unal.edu.co

---

## 1. INTRODUCTION

Research on dynamic systems has been applied to different fields such as biology, power converters, impact oscillators, mechanical systems, etc. where a large number of phenomena [1] of a non-linear nature [2, 3] are presented. Dynamic systems defined in pieces are very important topics of study in theoretical and experimental matters, being investigated in depth in recent years. An example of systems defined in pieces, are DC-DC voltage converters, which allow the control of output voltage from a given voltage source; that is, they act as bridges for energy transfers between sources and loads, both of direct current [4]. This leads naturally to the question of how to transfer energy from the source to the load with  $V_{in}$  amplitude, which needs a  $x_{1ref}$  voltage, with the minimum loss of power. Multiple applications are presented by these converters including power sources in computers, distributed power systems, power systems in electric vehicles, etc [5, 6]. Therefore, this study has been a source of research in the fields of dynamic systems. Power converters introduce a series of non-linearities in the switching process, which is why they have been studied as variable structure systems. In [7] controllers were designed in sliding mode to work with this type of converter. Later, Carpita [8] designed a controller based on a sliding surface given by a linear proportion of the error and the derivative of the error. These two results allow working with a robust, stable, and efficient controller. However, by generating a discontinuous action of this controller, a "chattering" phenomenon arises in the system [9], which implies an increase in the ripple and distortion at the exit.

With the purpose of eliminating the "chattering" phenomenon, several techniques have been proposed to find a control scheme that guarantees a fixed switching frequency. For example, in [7], it is proposed to synthesize a controller that guarantees a zero average of voltage error through a technique known as Zero Average Current Error (ZACE). Fossas and his colleagues proposed a new control technique for power converters in which an auxiliary output is set and a digital control action is defined that guarantees zero average in the auxiliary output in each iteration, maintaining a fixed frequency of commutation, robustness, and stability. This technique is known as ZAD (Zero Average Dynamics) and consists of the definition of a switching surface on which the system is evolved on average. In [10], it has been implemented making use of the switching surface  $s(x(t)) = (x_1(t) - x_{1ref}) + k_s(\dot{x}_1(t) - \dot{x}_{1ref})$ , where good results are shown in terms of robustness and low output error. In [11, 12] it is also applied to analyze the dynamics present in the boost converter to study present non-linear phenomena, driven by a center aligned pulse width modulation converter (CPWM).

In the present article, the ZAD technique has been implemented to control a SEPIC converter, which has been used to control boost and buck converters in previous Works [11, 13, 14]. A linear combination of the error in voltage and current has also been taken as the switching surface  $s(x(t)) = k_1(x_1(t) - x_{1ref}) + k_2(x_2(t) - x_{2ref}) + k_3(x_3(t) - x_{3ref}) + k_4(x_4(t) - x_{4ref})$  and from this, the calculation of duty cycle has been done with which the system is evolved in a period of time  $T$  [15]. Finally, bifurcations that arise in the evolution of 1-periodic orbits have been characterized and the presence of chaos has been determined from certain values of constants associated with the commutation surface, which were taken as bifurcation parameters [16, 17].

## 2. RESEARCH METHOD

An SEPIC converter [18] is a DC to DC converter belonging to the family of fourth-order converters [19]. This device can supply more or less voltage than the input voltage. The basic scheme of a SEPIC converter is shown in Figure 1, where  $V_{in}$  is the input voltage,  $i_1$  is the current in  $L_1$  inductor,  $S$  is the switch,  $D$  is the diode,  $v_1$  is the voltage in  $C_1$  capacitor,  $R$  is load resistance,  $i_2$  is the current in  $L_2$  inductor,  $v_2$  is the voltage in  $C_2$  capacitor. The basic principle of the SEPIC converter consists of two different states, depending on the state of the switch  $S$ .

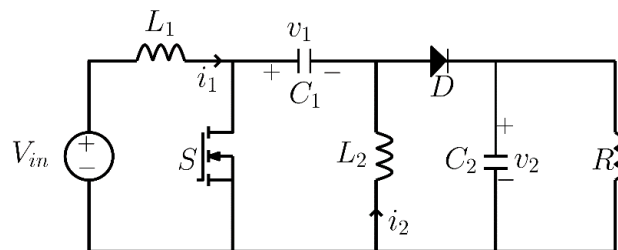


Figure 1. Basic scheme of an SEPIC converter

When switch  $S$  is closed, the status is *ON* and the input source  $V_{in}$  connects to  $L_1$  coil at the same time as the diode  $D$  is polarized inversely. As a consequence, the intensity that circulates through  $L_1$  inductance grows linearly, storing energy. In this situation, the  $C_1$  capacitor feeds the  $L_2$  inductor and the tension of  $C_2$  is delivered to the load. When switch  $S$  is open, the status *OFF* and the energy previously stored in  $L_1$  coil together with the input is transferred to the  $C_1$  input capacitor and the energy stored in the  $L_2$  inductor is transferred to  $C_2$  and to the load.

Two modes of operation are distinguished in the SEPIC converter, depending on the currents by the inductors canceled during the operation period  $T$ : Continuous Driving Mode (*MCC*) and Discontinuous Driving Mode (*MCD*). In this article, we will study the dynamics of the SEPIC converter in *MCC*. The dynamics of the SEPIC converter are governed by the solution of this system of differential equations:

$$\begin{aligned}
L_1 \frac{di_1}{d\tau} &= -(1-u)(v_1 + v_2) + V_{in} \\
C_1 \frac{dv_1}{d\tau} &= (1-u)i_1 - ui_2 \\
L_2 \frac{di_2}{d\tau} &= uv_1 - (1-u)v_2 \\
C_2 \frac{dv_2}{d\tau} &= (1-u)(i_1 + i_2) - \frac{v_2}{R}.
\end{aligned} \tag{1}$$

In this system,  $i_1$ ,  $v_1$ ,  $i_2$ , and  $v_2$  are status variables  $L_1$ ,  $L_2$ ,  $C_1$ ,  $C_2$ , and  $R$  are the parameters and  $u \in \{0,1\}$  is the control variable. In system (1), if  $u = 1$ , then SEPIC is *ON* (topology 1) and when  $u = 0$ , SEPIC is *OFF* (topology 2). Making the change of variables:

$$\begin{aligned}
x_1 &= \frac{i_1}{V_{in}} \sqrt{\frac{L_1}{C_1}} & x_2 &= \frac{v_1}{V_{in}} & x_3 &= \frac{i_2}{V_{in}} \sqrt{\frac{L_1}{C_1}} & x_4 &= \frac{v_2}{V_{in}} \\
t &= \frac{\tau}{\sqrt{L_1 C_1}},
\end{aligned} \tag{2}$$

if  $\alpha = \frac{L_2}{L_1}$ ,  $\beta = \frac{C_2}{C_1}$ , and  $\gamma = R \sqrt{\frac{C_1}{L_1}}$  are defined, then a dimensional system is obtained for the dynamics of the SEPIC converter:

$$\begin{aligned}
\dot{x}_1 &= -(1-u)(x_2 + x_4) + 1 \\
\dot{x}_2 &= (1-u)x_1 - ux_3 \\
\alpha \dot{x}_3 &= ux_2 - (1-u)x_4 \\
\beta \dot{x}_4 &= (1-u)(x_1 + x_3) - \frac{x_4}{\gamma},
\end{aligned} \tag{3}$$

where the new parameters of the system are  $\alpha$ ,  $\beta$ , and  $\gamma$ . Each topology of the system can be expressed in compact form by

$$\dot{\mathbf{x}} = \mathbf{A}_i \mathbf{x}(t) + \mathbf{b}, \tag{1}$$

where  $i \in \{1,2\}$  and

$$\mathbf{A}_1 = \begin{bmatrix} 0 & 0 & 0 & 0 \\ 0 & 0 & -1 & 0 \\ 0 & \frac{1}{\alpha} & 0 & 0 \\ 0 & 0 & 0 & -\frac{1}{\beta\gamma} \end{bmatrix}, \mathbf{A}_2 = \begin{bmatrix} 0 & -1 & 0 & -1 \\ 1 & 0 & 0 & 0 \\ 0 & 0 & 0 & \frac{-1}{\alpha} \\ \frac{1}{\beta} & 0 & \frac{1}{\beta} & -\frac{1}{\beta\gamma} \end{bmatrix}, \mathbf{b} = \begin{bmatrix} 1 \\ 0 \\ 0 \\ 0 \end{bmatrix}.$$

The solution of each topology can be expressed as

$$\mathbf{x}_i = \phi_i(t - t_0) \mathbf{x}(t_0) + \boldsymbol{\psi}_i(t - t_0), \tag{2}$$

where  $\phi_i(t - t_0) = e^{\mathbf{A}_i(t-t_0)}$  and  $\boldsymbol{\psi}_i(t - t_0) = \int_{t_0}^t e^{\mathbf{A}_i(t-\tau)} \mathbf{b} d\tau$

### 2.1. Pulse width modulation

The control scheme [20] that will be used in this study corresponds to center-aligned modulation by pulse width in such a way that a time interval  $[nT, (n+1)T]$  is divided into three subintervals, where the first and the last have the same length, as shown in Figure 2. Commutations are made according to the scheme  $\{1,0,1\}$  and, therefore, the system will operate as follows:

$$\dot{\mathbf{x}} = \begin{cases} \mathbf{A}_1 \mathbf{x} + \mathbf{b} & \text{si } nT \leq t \leq nT + \frac{d}{2} \\ \mathbf{A}_2 \mathbf{x} + \mathbf{b} & \text{si } nT + \frac{d}{2} \leq t \leq (n+1)T - \frac{d}{2} \\ \mathbf{A}_1 \mathbf{x} + \mathbf{b} & \text{si } (n+1)T - \frac{d}{2} \leq t \leq (n+1)T, \end{cases} \tag{6}$$

where  $T$  is the period,  $d$  is the duty cycle and the time during which the system is operated in status *ON*.

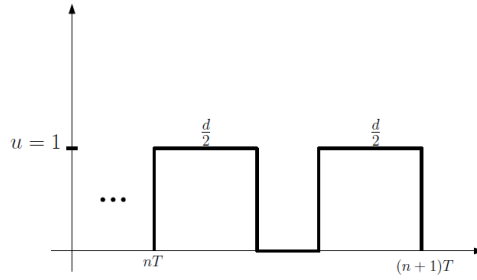


Figure 2. Symmetrical center pulse

After choosing the control scheme, we must decide how to calculate the time that the system must remain in conduction; that is, we must choose a criterion that allows us to calculate (period to period) the duty cycle  $d$ . In this paper, we will calculate it using ZAD (Zero Average Dynamics) control technique [2] and based on the fact that being a variable structure system, the principles of control in sliding modes can be applied in such a way that the error dynamic is zero on average in each iteration [21, 22].

**3. CONTROL STRATEGY**

**3.1. ZAD control strategy**

This technique consists of defining a switching surface  $s(\mathbf{x}(t)) = 0$  in which the system will evolve on average [12]. In this paper, the switching surface given by the equation  $s(\mathbf{x}(t)) = (x_1(t) - x_{1ref}) + k_s(\dot{x}_1(t) - \dot{x}_{1ref})$ , using this switching surface and the technical control ZAD, we obtain the next expression for the duty cycle:

$$d = \frac{2s(\mathbf{x}(nT)) + T\dot{s}_2(\mathbf{x}(nT))}{\dot{s}_2(\mathbf{x}(nT)) - \dot{s}_1(\mathbf{x}(nT))} \tag{7}$$

where  $d$  is a real number between 0 and  $T$ , if  $d < 0$  or  $d > T$ . Expression (7) is redefined, saying that the system is saturated. For this situation, the following selection is made in each period:

$$d = \begin{cases} 0 & \text{if } d \leq 0 \\ T & \text{if } d \geq T \end{cases} \tag{8}$$

**3.2. Poincaré map**

The Poincaré map of the SEPIC converter controlled with CPWM {1,0,1} and ZAD technique is given by the following:

1. If  $d_n \in (0, T)$  (duty cycle does not saturate)

$$\begin{aligned} P(\mathbf{x}_n, d_n) &= \phi_1\left(\frac{d_n}{2}\right)\phi_2(T - d_n)\phi_1\left(\frac{d_n}{2}\right)\mathbf{x}(nT) \\ &+ \phi_1\left(\frac{d_n}{2}\right)\phi_2(T - d_n)\psi_1\left(\frac{d_n}{2}\right) \\ &+ \phi_1\left(\frac{d_n}{2}\right)\psi_2(T - d_n) + \psi_1\left(\frac{d_n}{2}\right), \text{ and} \end{aligned} \tag{9}$$

2. If  $d_n = 0$  (duty cycle saturates)

$$P(\mathbf{x}_n, d_n) = \phi_2(T)\mathbf{x}(nT) + \psi_2(T) \tag{10}$$

3. If  $d_n = T$  (duty cycle saturates)

$$P(\mathbf{x}_n, d_n) = \phi_1(T)\mathbf{x}(nT) + \psi_1(T) \tag{11}$$

**4. BIFURCATIONS**

In this section, a study of the qualitative change of the SEPIC converter is made by varying one of the parameters associated with the switching surface. To characterize the type of bifurcation we find, we will use the bifurcation diagram, which is obtained from the Poincaré map given by the relations (9), (10), and (11), and proper values of the Jacobian matrix evaluated at equilibrium points of the system.

### 4.1. Flip bifurcation

The simulation described below is presented when we consider the SEPIC converter as a reducer; in addition, we take as reference values the vector  $(0.0544 \ 1 \ 0.1237 \ 0.44)^T$ . Figure 3 shows a configuration of the state variables for which there is a 1T-periodic orbit that goes from stable to unstable, which indicates a bifurcation point. The point of interest is when  $k_3 \in [40, 60]$ . The diagrams of these figures were obtained by varying  $k_3$  in the specified range with  $k_1 = 25$ ,  $k_2 = -15$ ,  $k_4 = -10$ ,  $T = 0.18$ ,  $\alpha = 0.2683$ ,  $\beta = 0.7021$ , and  $\gamma = 3.5583$ . Reviewing the eigenvalues of the Jacobian matrix associated with the Poincaré application in Table 1 and observing Figure 3, we find the resulting bifurcation is of the flip type [23] because one of these values goes from being stable to unstable, crossing through  $-1$  for a value of the parameter  $k_3 = 51.96$ .

This type of bifurcation is characterized by a period doubling; that is, the system goes from having a 1T-periodic orbit to having 2T-periodic orbits. Table 1 presents the values of the Poincaré map. An analysis of these allows confirmation that this is a flip-type bifurcation [24, 25] because the proper value that goes from stable to unstable does it crossing by  $-1$  in the interval  $k_3 \in (51.40, 52.30)$  as shown in Figure 4. This type of bifurcation occurs because the orbit 1T-periodic becomes unstable and an orbit 2 T-periodic is born, i.e., a period doubling occurs [12].

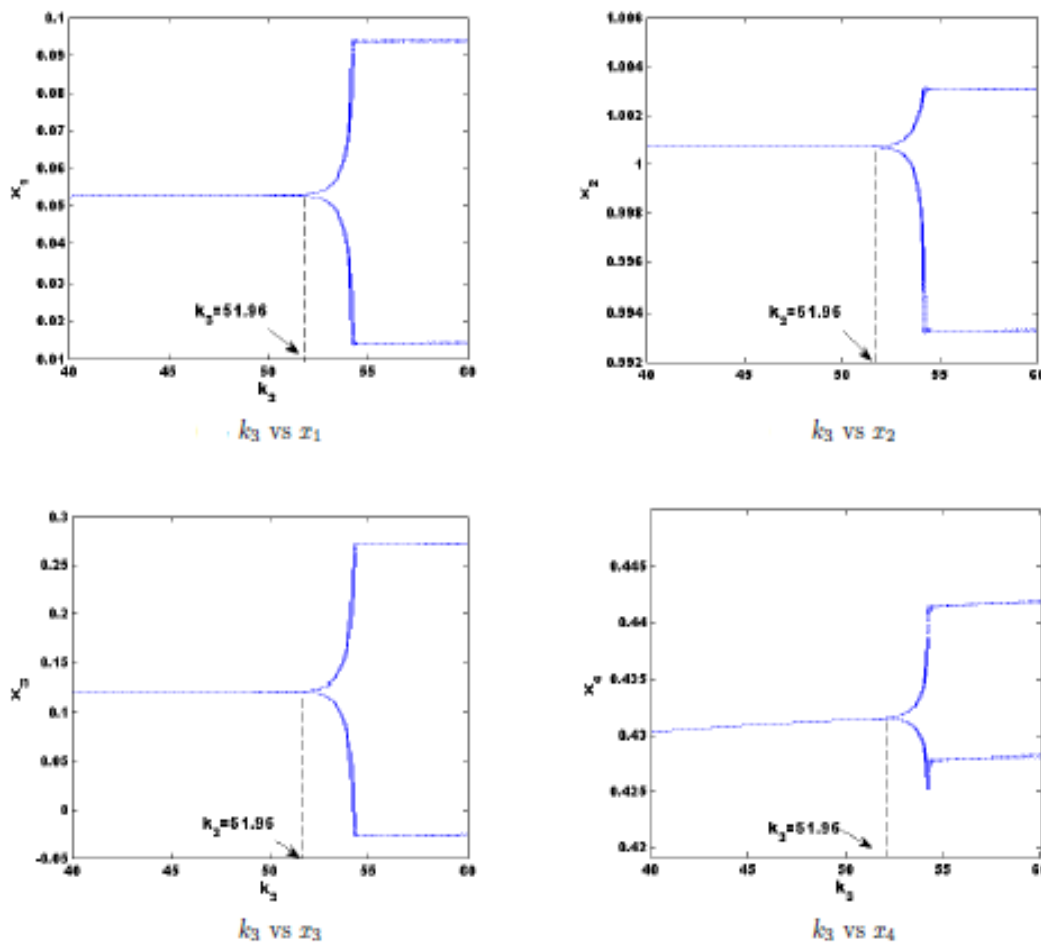


Figure 3. Bifurcation diagram varying  $k_3$

Table 1. Eigenvalues of the jacobian matrix near the stability limit when varying  $k_3$

$k_3$	$\lambda_1$	$\lambda_{2,3}$	$\lambda_4$
51.40	-0.99970	$0.98106 \pm 0.15499i$	0.95968
51.58	-0.99979	$0.98107 \pm 0.15495i$	0.95959
51.76	-0.99989	$0.98107 \pm 0.15492i$	0.95950
51.94	-0.99998	$0.98107 \pm 0.15489i$	0.95942
<b>52.12</b>	<b>-1.00008</b>	$0.98108 \pm 0.15485i$	0.95933
52.30	-1.00017	$0.981084 \pm 0.15482i$	0.95925

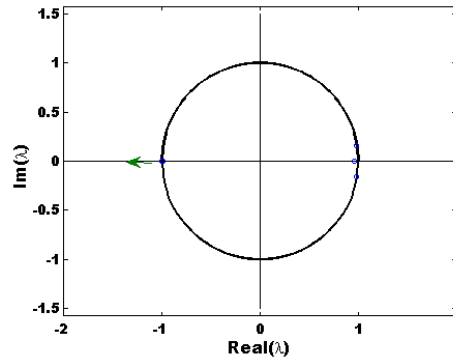


Figure 4. Graphic variation of eigenvalues by varying  $k_3$

**4.2. Neimar–saker bifurcation**

When  $k_1$  is varied in the interval  $[-10, -2]$  and we take as fixed values  $k_2 = 1, k_3 = -6, k_4 = 2.5, T = 0.18, \alpha = 0.2683, \beta = 0.7021, \gamma = 3.5583$ , and, as a condition, initial  $(1.1241 \ 1 \ 0.5621 \ 2)^T$ , we also find a bifurcation in the dynamics of the SEPIC converter as seen in Figure 5. In the bifurcation diagrams of Figure 5 a change in the dynamics of the system is observed, which is characteristic of a Neimar-Saker type bifurcation. To characterize this bifurcation, we analyze the evolution of the eigenvalues of the Jacobian matrix of the Poincaré map near the point of bifurcation  $k_1 = -2.42$ . We observe in Table 2 and Figure 6 that the complex and conjugated eigenvalues of the Poincaré application near the bifurcation point, its module approaches 1, which characterizes the Neimar–Saker-type bifurcation.

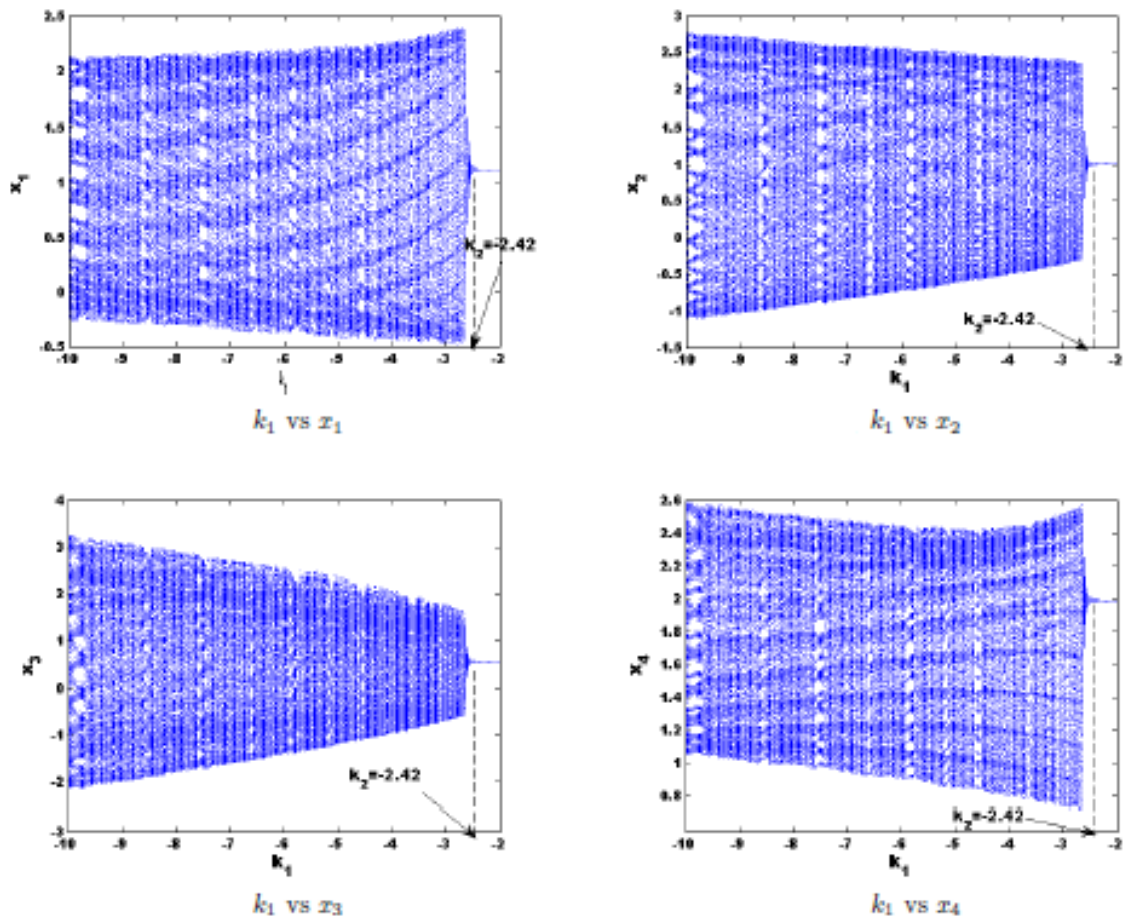


Figure 5. Bifurcation diagram varying  $k_1$

Table 2. Eigenvalues of the poincaré map near the stability limit when varying  $k_1$

$k_1$	$\lambda_1$	$\lambda_{2,3}$	$\lambda_4$
-3.0	-0.98014	$0.9918 \pm 0.1470i$	0.95786
-2.75	-0.97929	$0.9911 \pm 0.1447i$	0.96092
-2.5	-0.97843	$0.9902 \pm 0.1423i$	0.96426
-2.25	-0.97757	$0.9891 \pm 0.139i$	0.96792
-2.0	-0.97669	$0.9879 \pm 0.1372i$	0.97194

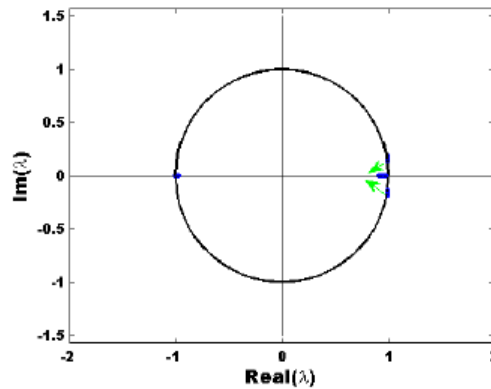


Figure 6. Graphic variation of eigenvalues by varying  $k_1$

**5. EXISTENCE AND CHAOS CONTROL**

To guarantee the presence of chaos in the system, we use the exponents of Lyapunov, which determine the proximity or divergence of two orbits that were initially close. The  $i$ -th Lyapunov exponent is given by the expression:

$$L_i = \lim_{k \rightarrow \infty} \left( \frac{1}{k} \sum_{n=0}^k \log |\lambda_i(JP(\mathbf{x}_n))| \right), \tag{12}$$

where  $\mathbf{x}_n$  is the  $i$ -th value of Poincaré map,  $JP$  its Jacobian, and  $\lambda_i$  is the  $i$ -th eigenvalue of  $JP$ . The presence of a positive Lyapunov exponent in a system whose trajectories evolve within a finite zone of the state space guarantees chaotic behavior [26]. On the other hand, the sum of all Lyapunov exponents in a chaotic attractor must be negative [27].

To determine the presence of chaos [16, 28] and its respective control, we will use the values with which the flip bifurcation was obtained. Figure 7 shows the existence of positive Lyapunov exponents for values of  $k_3$  greater than 51.96 . Additionally, Figure 3 shows that for values of  $k_3 \in (51.40, 52.30)$ , the system evolves in a bounded region of the state space. Therefore, we can see that the system presents chaotic behavior for values of  $k_3$  greater than 51.96.

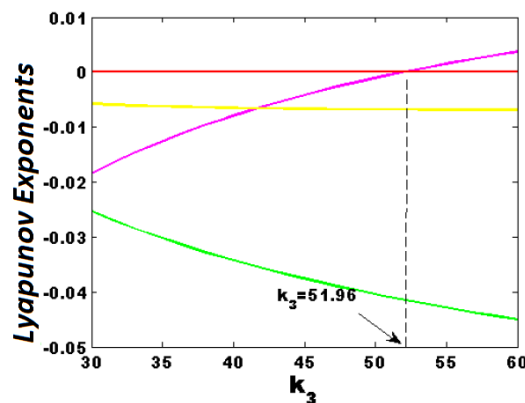


Figure 7. Lyapunov exponents by varying  $k_3$

**5.1. Chaos control with FPIC technique**

Because our system is non-autonomous, it is excited with an external signal  $u$ . Any method of chaos control must stabilize the unstable orbits, and for this it must necessarily assure that proper values of the Jacobian matrix of the Poincaré map are within the unit circle (stability border). In this sense, several control strategies have been designed. To control the chaos presented by the SEPIC converter with ZAD, we use the FPIC (Fixed Point Induced Control) technique [29], which was designed by [14] and has been used numerically in [13, 30].

This is based on the continuity of proper values theorem and helps stabilize period one or more orbits in unstable and/or chaotic systems and does not require the measurement of state variables. It forces the system to evolve to the fixed point; therefore, it is necessary to have prior knowledge of the control signal equilibrium point. The equilibrium point obtained for the system is given by the transposed vector:

$$\mathbf{x}^* = \left( \frac{x_{4ref}^2}{\gamma}, 1, \frac{x_{4ref}}{\gamma}, x_{4ref} \right)^t,$$

that corresponds to a steady-state duty cycle

$$d^* = T \frac{x_{4ref}}{1+x_{4ref}} \tag{13}$$

The duty cycle  $d_{ZF}$  is to apply ZAD and FPIC control techniques is given by:

$$d_{ZF} = \frac{d+Nd^*}{N+1}, \tag{14}$$

where  $d$  is determined by (7) and  $d^*$  by (13).

Next we apply the FPIC technique to the dynamics of the SEPIC converter. Figures 8 (a) shows that by choosing  $N = 0.003$ , the area in which the system exhibits chaotic behavior decreases. Figure 8 (b) shows that for the FPIC constant  $N = 0.005$  the area in which the system exhibits chaotic behavior continues to decrease. Finally in Figure 8 (c) when the FPIC constant  $N = 0.006$  the area in which the system exhibits chaotic behavior has almost completely disappeared.

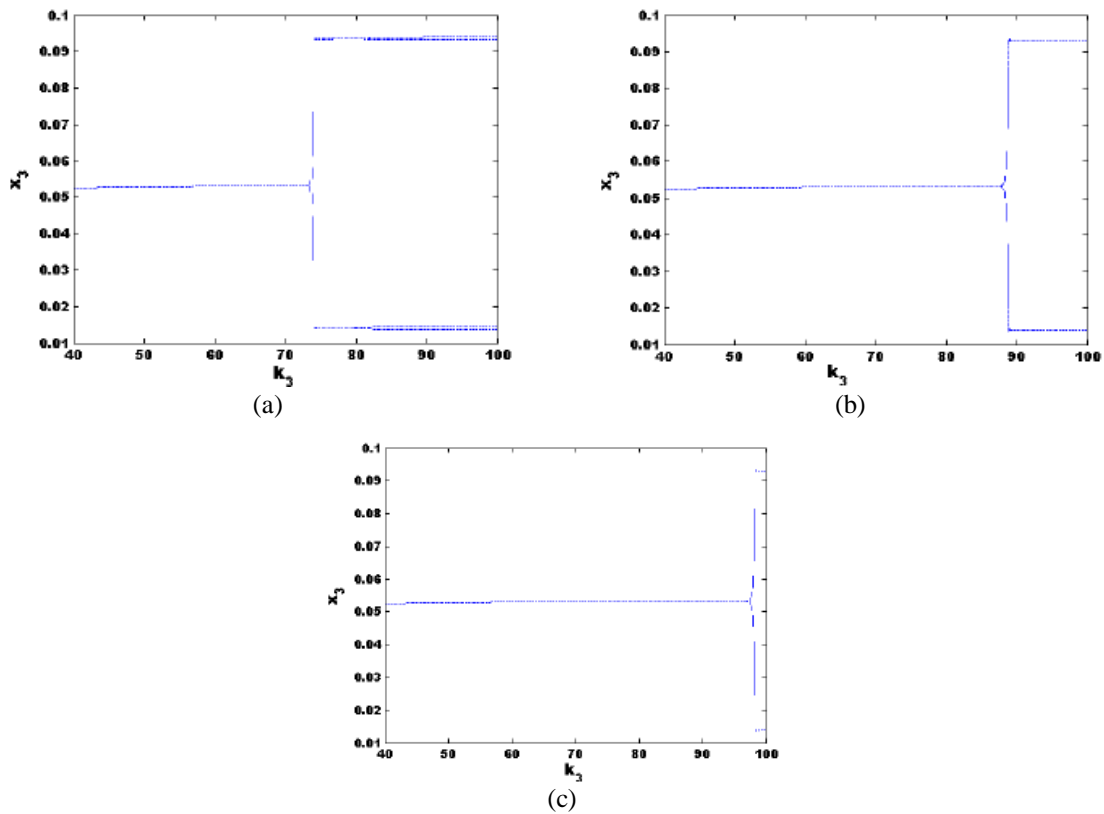


Figure 8. Bifurcation diagram varying  $k_3$  with FPIC control (a)  $N = 0.003$ , (b)  $N = 0.005$ , (c)  $N = 0.006$

## 6. CONCLUSION

By analyzing the dynamics of the SEPIC converter numerically using the ZAD technique with CPWM, we can observe the presence of non-linear phenomena such as quasi-periodicity and chaos. The presence of bifurcations was detected by varying the parameters  $k_1$  and  $k_3$  associated to the switching surface, being the flip and Neimar–Saker bifurcations, respectively. Chaotic behavior can be controlled by introducing the FPIC technique. However, it is important to see how the FPIC technique influences other behaviors of the system, such as regulation.

## ACKNOWLEDGEMENTS

This paper was supported by the Universidad Nacional de Colombia, Sede Medellín under the projects HERMES- 36911 and HERMES- 34671. The authors thank the School of Physics for their valuable support to conduct this research.

## REFERENCES

- [1] N. Toro-García, Y. Garcés-Gómez, and F. Hoyos, “Discrete and Continuous Model of Three-Phase Linear Induction Motors ‘LIMs’ Considering Attraction Force,” *Energies*, vol. 12, no. 4, p. 655, Feb. 2019.
- [2] F. E. Hoyos, J. E. Candelo, and J. A. Taborda, “Selection and validation of mathematical models of power converters using rapid modeling and control prototyping methods,” *Int. J. Electr. Comput. Eng.*, vol. 8, no. 3, p. 1551, Jun. 2018.
- [3] K. Aihara and H. Suzuki, “Theory of hybrid dynamical systems and its applications to biological and medical systems,” *Philos. Trans. R. Soc. A Math. Phys. Eng. Sci.*, vol. 368, no. 1930, pp. 4893–4914, Nov. 2010.
- [4] R. Palanisamy, K. Vijayakumar, V. Venkatachalam, R. M. Narayanan, D. Saravanakumar, and K. Saravanan, “Simulation of various DC-DC converters for photovoltaic system,” *Int. J. Electr. Comput. Eng.*, vol. 9, no. 2, p. 917, Apr. 2019.
- [5] D. Sattianadan, K. Saravanan, S. Murugan, N. Hari, and P. Venkadesh, “Implementation of quasi-z source inverter for grid connected PV based charging station of electric vehicle,” *Int. J. Power Electron. Drive Syst.*, vol. 10, no. 1, p. 366, Mar. 2019.
- [6] C. Mahmoudi, F. Aymen, and S. Lassaad, “Smart database concept for Power Management in an electrical vehicle,” *Int. J. Power Electron. Drive Syst.*, vol. 10, no. 1, p. 160, Mar. 2019.
- [7] E. Fossas, R. Griño, and D. Biel, “Quasi-Sliding control based on pulse width modulation, zero averaged dynamics and the L2 norm,” in *Advances in Variable Structure Systems - 6th IEEE International Workshop on Variable Structure Systems*, pp. 335–344, 2000.
- [8] M. Carpita and M. Marchesoni, “Experimental study of a power conditioning system using sliding mode control,” *IEEE Trans. Power Electron.*, vol. 11, no. 5, pp. 731–742, Sep. 1996.
- [9] A. Abrishamifard, A. Ahmad, and M. Mohamadian, “Fixed Switching Frequency Sliding Mode Control for Single-Phase Unipolar Inverters,” *IEEE Trans. Power Electron.*, vol. 27, no. 5, pp. 2507–2514, May 2012.
- [10] F. Angulo, J. E. Burgos, and G. Olivar, “Chaos stabilization with TDAS and FPIC in a buck converter controlled by lateral PWM and ZAD,” in *2007 Mediterranean Conference on Control & Automation*, pp. 1–6, 2007.
- [11] D. D. C. Vergara Perez, S. C. Trujillo, and F. E. Hoyos Velasco, “Period Addition Phenomenon and Chaos Control in a ZAD Controlled Boost Converter,” *Int. J. Bifurc. Chaos*, vol. 28, no. 13, p. 1850157, Dec. 2018.
- [12] A. Amador, S. Casanova, H. A. Granada, G. Olivar, and J. Hurtado, “Codimension-Two Big-Bang Bifurcation in a ZAD-Controlled Boost DC-DC Converter,” *Int. J. Bifurc. Chaos*, vol. 24, no. 12, p. 1450150, Dec. 2014.
- [13] Hoyos, Candelo-Becerra, and Hoyos Velasco, “Model-Based Quasi-Sliding Mode Control with Loss Estimation Applied to DC–DC Power Converters,” *Electronics*, vol. 8, no. 10, p. 1086, Sep. 2019.
- [14] F. Hoyos Velasco, J. Candelo-Becerra, and A. Rincón Santamaría, “Dynamic Analysis of a Permanent Magnet DC Motor Using a Buck Converter Controlled by ZAD-FPIC,” *Energies*, vol. 11, no. 12, p. 3388, Dec. 2018.
- [15] A. Rincón, F. Angulo, and F. Hoyos, “Controlling a DC Motor through Lypaunov-like Functions and SAB Technique,” *Int. J. Electr. Comput. Eng.*, vol. 8, no. 4, p. 2180, Aug. 2018.
- [16] F. E. Hoyos Velasco, N. Toro-García, and Y. A. Garcés Gómez, “Adaptive Control for Buck Power Converter Using Fixed Point Inducting Control and Zero Average Dynamics Strategies,” *Int. J. Bifurc. Chaos*, vol. 25, no. 04, p. 1550049, Apr. 2015.
- [17] F. E. Hoyos, D. Burbano, F. Angulo, G. Olivar, N. Toro, and J. A. Taborda, “Effects of Quantization, Delay and Internal Resistances in Digitally ZAD-Controlled Buck Converter,” *Int. J. Bifurc. Chaos*, vol. 22, no. 10, p. 1250245, Oct. 2012.
- [18] B. Slimane, A. Othmane, and A. Ben Abdelkader, “Unified Power Quality Conditioner Supplied by Fuel Cell System Via SEPIC Converter,” *Int. J. Power Electron. Drive Syst.*, vol. 10, no. 1, p. 178, Mar. 2019.
- [19] Tasi-Fu Wu and Yu-Kai Chen, “Modeling PWM DC/DC converters out of basic converter units,” *IEEE Trans. Power Electron.*, vol. 13, no. 5, pp. 870–881, Sep. 1998.
- [20] F. E. Hoyos, J. E. Candelo-Becerra, and N. Toro, “Numerical and experimental validation with bifurcation diagrams for a controlled DC–DC converter with quasi-sliding control,” *TecnoLógicas*, vol. 21, no. 42, pp. 147–167, May 2018.
- [21] J. A. Taborda, “Análisis de bifurcaciones en sistemas de segundo orden usando pwm y promediado cero de la dinámica del error,” Universidad Nacional de Colombia - Sede Manizales, 2006.

- [22] J. E. C.-B. Fredy E. Hoyos, Carlos I. Hoyos, "DC-AC power inverter controlled analogically with zero hysteresis," *Int. J. Electr. Comput. Eng.*, vol. 9, no. 6, pp. 4767–4776, 2019.
- [23] J. Knight, S. Shirsavar, and W. Holderbaum, "An improved reliability cuk based solar inverter with sliding mode control," *IEEE Trans. Power Electron.*, vol. 21, no. 4, pp. 1107–1115, Jul. 2006.
- [24] R. Yu and X. Zhou, "Flip Bifurcation of a Class of Discrete-time Neural Networks," in *2009 WRI Global Congress on Intelligent Systems*, pp. 91–95, 2009.
- [25] A. Kavitha and G. Uma, "Bifurcation Analysis of DC-DC Converters using Discrete Time Model," in *2008 Joint International Conference on Power System Technology and IEEE Power India Conference*, pp. 1–7, 2008.
- [26] J. A. Taborda, S. Santini, M. di Bernardo, and F. Angulo, "Active Chaos Control of a Cam-Follower Impacting System using FPIC Technique," *IFAC Proc. Vol.*, vol. 42, no. 7, pp. 327–332, 2009.
- [27] J. I. Ramos, "Practical Numerical Algorithms for Chaotic Systems," *Appl. Math. Model.*, vol. 15, no. 11–12, pp. 663–664, Nov. 1991.
- [28] A. Sambas, S. Vaidyanathan, M. Mamat, M. A. Mohamed, and M. S. WS, "A New Chaotic System with a Pear-shaped Equilibrium and its Circuit Simulation," *Int. J. Electr. Comput. Eng.*, vol. 8, no. 6, p. 4951, Dec. 2018.
- [29] H. Tirandaz, M. Ahmadnia, and H. Tavakoli, "Adaptive Projective Lag Synchronization of T and Lu Chaotic Systems," *Int. J. Electr. Comput. Eng.*, vol. 7, no. 6, pp. 3446–3453, 2017.
- [30] F. Angulo, G. Olivar, J. Taborda, and F. Hoyos, "Nonsmooth dynamics and FPIC chaos control in a DC-DC ZAD-strategy power converter," in *ENOC*, pp. 1–6, 2008.

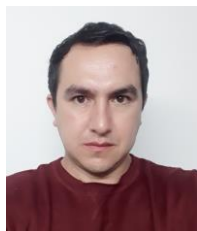
## BIOGRAPHIES OF AUTHORS



**Aquiles José Morelo Sanchez:** received his B.S. degree in Matemáticas in 1999, M.S in Sciences-Applied Mathematics in 2015, rector of the Educational Institucion Canutalito, Ovejas-Sucre, Colombia, E-mail: ajmorelos@unal.edu.co. His research interests include didactics in the teaching of mathematics and dynamic systems.



**Simeon Casanova Trujillo:** received his B.S. degree in Mathematics and Physics in 1993, M.S in Mathematics in 1997 and Ph.D in Automation in 2011. Dr. Casanova is currently an Associate Professor of the Exact and Natural Sciences Faculty, at National University of Colombia, at Manizales, Colombia. His research interests include nonlinear dynamics analysis, control of nonsmooth systems, and differentiability in topological groups.



**Fredy Edimer Hoyos:** received his BS and MS degree from the National University of Colombia, at Manizales, Colombia, in Electrical Engineering and Industrial Automation, in 2006 and 2009, respectively, and an Industrial Automation Ph.D. in 2012. Dr. Hoyos is currently an Associate Professor of the Science Faculty, School of Physics, at National University of Colombia, at Medellin, Colombia. His research interests include nonlinear control, system modeling, nonlinear dynamics analysis, control of nonsmooth systems, and power electronics, with applications extending to a broad area of technological processes. Dr. Hoyos is an Associate Researcher in Colciencias and member of the Applied Technologies Research Group (GITA) at the Universidad Nacional de Colombia. <https://orcid.org/0000-0001-8766-5192>